

Physically Based Simulation of Potential Effects of Carbon Dioxide–Altered Climates on Groundwater Recharge

Timothy R. Green,* Bryson C. Bates, Stephen P. Charles, and P. Mick Fleming

Increasing concentrations of atmospheric CO₂ will alter regional rainfall and evapotranspiration regimes that drive groundwater recharge. Improved methods of simulation and analysis are needed for assessing the potential sensitivities of soil–water–vegetation systems to climate change. This study demonstrates methods for generating climates and simulating soil–water and vegetation dynamics in response to current and double CO₂ climate sequences. Climate change scenarios came from dynamic equilibrium (constant CO₂) runs of a general circulation model (GCM). Based on historical climate and GCM output, a stochastic point weather generator produced realizations of the cross-correlated daily climate variables. A numerical model of infiltration, variably saturated flow, and evapotranspiration produced temporal distributions of groundwater recharge rates for various soil–vegetation environments. Climate change scenarios were simulated for two climatic zones in Australia: subtropical (North Stradbroke Island, Queensland) and Mediterranean (Gnangara, Swan Coastal Plain, Western Australia) having summer- and winter-dominated rainfall regimes, respectively. In these simulations, groundwater recharge values were affected by the dynamic growth and senescence of vegetation, as changes in temperature and rainfall regimes affected growth rates and leaf areas. The temperature regime dominated the hydrologic response in the Mediterranean climate, and the rainfall frequency–duration regime dominated in the subtropical climate. For the simulated Mediterranean climate change (14% rainfall increase), changes in mean recharge values ranged from –34% to +119%, while subtropical climate change (37% rainfall increase) caused increases from 74 to > 500%. Changes in mean recharge rate, interannual variability, and temporal persistence were related to the soil and vegetation characteristics. The model was useful for quantifying complex, nonlinear responses to climate change that require further exploration.

ABBREVIATIONS: ET, evapotranspiration; GCM, general circulation model; PET, potential evapotranspiration; RCM, regional climate model; SVAT, soil–vegetation–atmosphere transfer; VPD, vapor pressure deficit.

Despite the critical importance of groundwater resources in many parts of the world, there have been very few direct studies of the effect(s) of global warming on groundwater recharge.

Watson et al. (1996, p. 336)

Although the effects . . . on groundwater resources are not adequately understood at present, they cannot be ignored.

Watson et al. (1998, p. 122)

Groundwater is the major source of water across much of the world, particularly in rural areas in arid and semiarid regions, but there has been very little research on the potential effects of climate change.

McCarthy et al. (2001, p. 199)

T.R. Green, USDA-ARS, Fort Collins, CO 80526; B.C. Bates and S.P. Charles, CSIRO Land and Water, Floreat, Western Australia 6014, Australia; P.M. Fleming, CSIRO Land and Water, Canberra, ACT 2601, Australia (retired). Received 9 July 2006. *Corresponding author (tim.green@ars.usda.gov).

Vadose Zone J. 6:597–609
doi:10.2136/vzj2006.0099

© Soil Science Society of America
677 S. Segoe Rd. Madison, WI 53711 USA.
All rights reserved. No part of this periodical may be reproduced or transmitted in any form or by any means, electronic or mechanical, including photocopying, recording, or any information storage and retrieval system, without permission in writing from the publisher.

As these quotations from the Intergovernmental Panel on Climate Change illustrate, there has been a continuing need to develop methods for assessing the potential effects of CO₂–altered climates on aquifer recharge. An editorial article in *Ground Water* (Sophocleous, 2004) confirmed the general need: “Although aquifers are generally sensitive to changes in recharge, little work has been done on the impacts of climate change on particular aquifers.” Furthermore, the dynamics of groundwater systems in response to human and climatic stresses require further attention (Alley et al., 2002).

Groundwater is a valuable resource in many parts of the world and particularly in arid to subhumid regions such as much of Australia. For water supply and environmental issues, the hydrologic fluxes of interest include temporal variability in groundwater recharge rates and the long-term yield (both human-induced and natural groundwater discharge) of the aquifers.

In the last several years, researchers have begun to estimate potential impacts of climate change on regional groundwater resources around the world. Simulation studies were performed on regions in Texas (Loáiciga et al., 2000), southwest Canada and northwestern USA (Scibek and Allen, 2006), and northeastern Germany (Wessolek and Asseng, 2006). These studies vary in terms of methods of simulating climates and hydrology, results of groundwater sensitivities to climate, and interpretations of how such results could be applied. Other approaches include paleo-recharge estimation using tracer methods, including isotopic data from Jordan (Bajjali and Abu-Jaber, 2001) and from north Africa and Italy (Zuppi and Sacchi, 2004) and borehole temperatures in Japan (Taniguchi, 2002).

We present here an approach and case studies for simulating the potential effects of climate change associated with doubling historical concentrations of carbon dioxide in the atmosphere. The general method involves simulation of CO₂-altered climates using a GCM, generation of daily weather variables using a stochastic daily weather generator based on historical data and the GCM results, and numerical simulation of rainfall infiltration, variably saturated flow (one-dimensional), and evapotranspiration, producing time series of daily deep drainage (a surrogate for groundwater recharge) for various soil-vegetation environments.

Details of the context for the present approach and contrast with alternative methods may be gained from recent literature reviews (Overgaard et al., 2006; Xu et al., 2005). Others have used regional climate models (RCMs) to downscale GCM results, and soil-vegetation-atmosphere transfer (SVAT) schemes have been coupled to RCMs. The prior emphasis has been on surface water or shallow soil water (e.g., Bell et al., 2007), in contrast to the present focus on deep drainage below the root zone to address groundwater recharge. To our knowledge, none of the RCM-SVAT models provide equivalent physically based simulations of water and energy including plant dynamics.

Plant water use (transpiration) is a critical component of the water budget, along with evaporation needed to compute groundwater recharge. Dooge (1992, p. 2683) noted that "meaningful scenarios of hydrologic prediction and climate prediction are not possible without an understanding of vegetation response." Thus, the present model includes effects of dynamic plant growth and respiration (including simulated changes in leaf area and root density) on transpiration and deep drainage. The approach presented here demonstrates the use of physically based climate and soil-plant-water models to explore previously unquantified sensitivities of groundwater recharge to potential climate change, including simulated plant dynamics.

Description of the Study Sites

Two sites in Australia (Fig. 1) with important groundwater resources were selected to demonstrate the present methods. The first site, North Stradbroke Island (referred to here as Stradbroke) near Brisbane on the east coast of Queensland, has a subtropical climate (Green et al., 1997). The second site is the Gngangara Mound (unconfined aquifer; referred to here as Gngangara) on the Swan Coastal Plain north of Perth, Western Australia, with a Mediterranean climate. Mean monthly values of historical rainfall and temperature are shown in Fig. 1 for each site.

Stradbroke is located about 40 km offshore from Brisbane in the eastern state of Queensland, Australia. It stretches about 32 km from north to south with an average latitude of approximately 27.5 degrees south. The island is a massive sand dune rising to

229 m above sea level over weathered rock (primarily Cenozoic deposits, with lesser amounts of Mesozoic sandstone, shale and tuff, and Paleozoic greenstone) to depths of over 90 m below sea level on the eastern side of the island. The dunes consist of fine to medium quartz grains. Deposits of silt-size particles and organic material form the base of inland lakes and swamps (Laycock, 1975). Because depths to the main water-table aquifer exceed 50 m over most of the inland areas where natural recharge occurs, no interaction with groundwater is considered in this study. The sand dunes are covered primarily by mixed forests, dominated by eucalyptus trees. The most common species are Blue Gum (*Eucalyptus tereticornis*) and scribbly gum (*E. signata*). Dunes in sand mining areas are stabilized by revegetating with perennial grasses. The climate on Stradbroke is subtropical, and summer rainfall is dominated by extratropical depressions and the southerly penetration of tropical cyclones. We used the continuously observed daily weather data from 1972 to 1991 at the Brisbane Airport (27° 25' S, 153° 5' E, elevation 6 m) for generating stochastic daily weather variables. The mean annual rainfall for this period was 1130 mm, and the mean annual potential evapotranspiration (PET) was approximately 1500 mm.

Gngangara is an unconfined, sandy aquifer located on the Swan Coastal Plain north of Perth in Western Australia (WAWA, 1987). It is centered at approximately 31° 40' S, 115° 50' E and covers an area of approximately 2200 km². The landscape is covered primarily by mixed forests, dominated by *Banksia* woodland and eucalyptus forest (Farrington et al., 1990). Approximately 10% of the area is covered with exotic pine plantations of various ages and densities (a basal area of 11 m² ha⁻¹ is the target), as well as cleared grasslands. Approximately 1 to 2% of the total

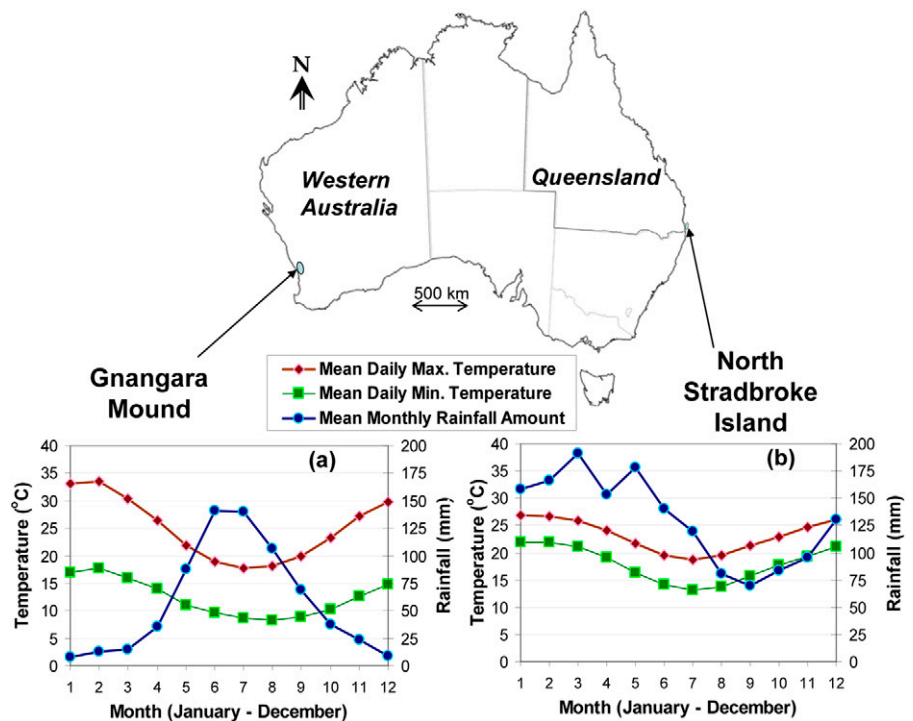


FIG. 1. Locations of study sites in Australia with plots of historical mean monthly rainfall amounts and mean monthly values of daily maximum and minimum temperatures at weather stations: (a) Pearce Air Force Base (-31.6669 degrees S, 116.0189 degrees E; years: 1937-2004) representing Gngangara, and (b) Cape Moreton Lighthouse (-27.0314 degrees S, 153.4661 degrees E; years: 1869-2004) representing Stradbroke. Data were downloaded from the Australian Bureau of Meteorology at <http://www.bom.gov.au/climate/averages/>.

land area is under intensive agriculture for vegetable production. The climate is Mediterranean with cool, wet winters and hot, dry summers. We used the continuously observed daily weather data from 1975 to 1991 at Pearce Air Force Base (31° 40' S, 116° 1' E, elevation 40 m) for generating stochastic daily weather variables. The mean annual rainfall for this period was 642 mm, and the mean annual PET was approximately 1400 mm.

In both locations, infiltration rates through the sandy soils can be very high, and much of the water used by humans in coastal areas is pumped from shallow aquifers. Furthermore, groundwater discharge to wetlands affects the health of ecosystems in these groundwater-controlled environments. Only recharge sites with relatively deep water table conditions (>5 m for grasses and >25 m for trees) were considered in this paper. Soils were assumed to be homogeneous with depth, although vertical heterogeneity could be incorporated using water, vegetation, energy, and solutes (WAVES) model, if known.

Materials and Methods

A sequence of simulation models was used to simulate the climate scenarios, vegetation response, soil moisture, infiltration, and deep drainage to groundwater (i.e., “recharge”):

1. CSIRO9 (Mark 1) General Circulation Model (McGregor et al., 1993).
2. MWGEN (Modified WGEN) stochastic daily point weather generator (after Bates et al., 1994).
3. WAVES soil-vegetation-atmosphere numerical model (Zhang et al. (1996) with minor modifications).

The flow of information is shown schematically in Fig. 2. Each component of the modeling framework is described below. In the present simulations, information flows in only one direction, and there are no feedbacks between the land surface conditions and the generated daily weather variables.

Models for Generating Climate Scenarios

The climate change scenarios studied here are based on historical records and simulations of the general circulation of the atmosphere. Here, we refer to the recent historical record as the “current” climate with an average atmospheric CO₂ concentration of 330 ppmv. Atmospheric CO₂ concentrations have risen almost linearly from about 330 ppmv in the 1970s to about 380 ppmv presently, compared with preindustrial levels of about 280 ppmv (Holper, 2002). The simulated climate data come from 24-yr dynamic equilibrium runs for the historical climate (assuming a constant CO₂ concentration of 330 ppmv) and doubled CO₂ (660 ppmv) climate. The procedure considers (i) changes in the distribution of precipitation amounts and frequency of precipitation events, (ii) changes in the daily means of temperature and global solar radiation series, (iii) effects of inter-annual climate variability as well as long-term climate changes, and (iv) preservation of the cross-correlation structure between climate variables (Bates et al., 1994).

General Circulation Model

McGregor et al. (1993) described the spectral GCM used in this study (CSIRO9 Mark 1). The model operates with nine ver-

tical levels in the atmosphere and a horizontal resolution of about 300 km by 600 km. GCM simulations provide daily values for 30 climatic variables, including precipitation, temperature, and global solar radiation. These output variables provide information on possible modifications of the frequency and distribution of rainfall events and potential evapotranspiration.

We first selected CSIRO9 GCM grid cells (300 × 600 km) that either contained the Gngangara and Stradbroke sites or an adjacent cell that best matched the statistics of the historical records. The changes between GCM simulations for current (Climate 1) and double CO₂ (Climate 2) conditions at these cells were used to estimate changes in MWGEN parameter values below. Thus, the simulation approach was used to generate steady-state climate “scenarios” rather than “projections” of transient climate change under different greenhouse gas emission scenarios (McCarthy et al., 2001).

Subsequent work has shown that transient GCM projections have a stronger drying signal for winter rainfall in southern Australia than the scenarios generated by CSIRO9 GCM for our simulations. The evolution of Australian winter rainfall projections can be traced through the CSIRO Climate Change Scenarios reports. In 1992 they reported a -20 to +20% change projected by 2070 (CSIRO, 1992). In 1996 they reported a change of -20 to 0%. (CSIRO, 1996). In 2001 they reported that the range of change for the southwest of western Australia based on coupled models in CSIRO (1996) was -8 to 0% for 2030 and that the current projections were -20 to +4% (CSIRO, 2001; Hennessy and Whetton, 2001).

More recently, Hennessy et al. (2006) published projections for 2030 that confirm a high degree of uncertainty associated with the magnitude of projected seasonal trends, including winter drying. Climate models producing drying trends will be used in future research for comparison but are beyond the scope of the current research, which focuses on methods for assessing dynamic sensitivities of groundwater recharge to simulated climate change scenarios.

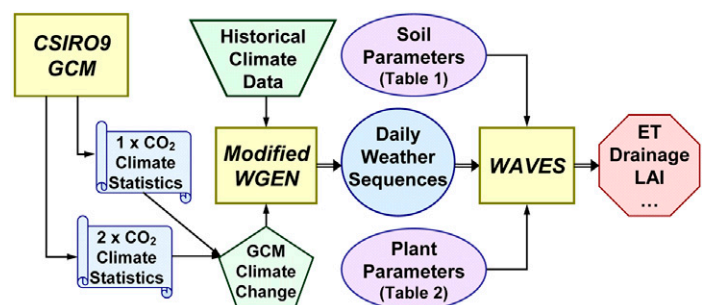


FIG. 2. Modeling framework for the flow of information at a given study site. Arrows with double lines indicate information passed for both climate scenarios at each site. Bates et al. (1994) provided further details regarding the generation of synthetic sequences of daily weather variables, including rainfall amount, temperature, and global solar radiation, which were inputs to the WAVES model for each climate scenario here. Outputs from WAVES include components of evapotranspiration (ET), drainage from the bottom soil boundary (equivalent to groundwater recharge reported here), leaf area index (LAI), and other variables not evaluated here, such as soil water content.

Stochastic Point Weather Generator

The stochastic weather generator used in this study is based on the WGEN model (Richardson and Wright, 1984). Subsequently, Wilks (1992) presented a method for adapting stochastic daily weather models (fitted to historical weather series) to generate synthetic series for future climates. The model parameters were adjusted to be consistent with the changes in monthly statistics from GCM runs for current and double CO₂ conditions. Artificial “drizzle” in GCM results remained an issue affecting rainfall frequency at the lowest amounts, but the use of differences in GCM runs (Fig. 2) helped to cancel out such GCM artifacts.

Following this type of approach, the modified model (MWGEN) also includes higher-order harmonics for temperature and an atmospheric transmission model for solar radiation to calculate the clear day maximum at the ground surface (Fleming, 1987). Ground surfaces were assumed to be flat for these analyses. For each calendar month, a generalized beta distribution was fitted to the daily residuals (i.e., differences between the clear day maximum and observations) for wet and dry days. Occurrence of either wet or dry days was determined by a two-state, lag-1 Markov model. The rainfall amount distribution for wet days was represented by a highly skewed Gamma distribution. Two climate scenarios (1000 yr each of daily data) were generated for each study site using MWGEN. The climatic variables simulated are precipitation occurrence and amount, maximum and minimum temperature, and global solar radiation. Further details regarding the generation of daily weather sequences for each climate scenario were given by Bates et al. (1994).

Soil Water and Vegetation Model

The WAVES (water, vegetation, energy, and solutes) model (Zhang et al., 1996) simulates infiltration and vertical redistribution of water through soil columns under dynamic plant cover. The computed “deep drainage” is equated with groundwater recharge. The model is used here with literature values of parameter for various components, except as noted. No data were available for site-specific calibration, so the model was not calibrated to present conditions.

Vertical Water Movement

Richards’ equation for variably saturated flow in one dimension (vertical) was solved numerically using a finite difference method in WAVES (Dawes and Short, 1993; Dawes and Zhang, 1998). The solution technique is very efficient and numerically stable, owing to the methods outlined by Ross and Bristow (1990) and Dawes and Zhang (1998) using:

1. The mixed form of Richards’ equation to conserve mass (Milly 1985),
2. Implicit time iteration allowing relatively long time steps (Brutsaert, 1971), and
3. Kirchhoff integral transform of the matric potential allowing relatively large space increments (Short et al., 1996).

The soil hydraulic properties were represented by the Broadbridge and White (1988) functions, where soil water retention was represented analytically as

$$\Psi(\Theta) = \frac{(\Theta - 1)}{\Theta} - \frac{1}{C} \ln \left[\frac{C - \Theta}{\Theta(C - 1)} \right] \quad [1]$$

where $\Psi = \psi/\lambda_c$ and $\Theta = (\theta - \theta_o)/(\theta_s - \theta_o)$, ψ is the matric potential, θ is the volumetric water content, λ_c is the capillary length, θ_s and θ_o are the saturated and residual volumetric water contents, respectively, and C is a fitting parameter which is also related to one of two parameters in the soil–water diffusivity function of Knight and Philip (1979).

Boundary and Initial Conditions

The surface boundary condition is generally rainfall infiltration with ponding occurring only for extreme events on finer textured soils. Any simulated runoff is subtracted from the water balance without further interaction. Surface runoff was an insignificant portion of the total rainfall in all cases, so it is not discussed below. The soils drain by gravity at the base of the simulated columns (5 m for grasses and 25 m for trees), and the computed “deep drainage” is equated with groundwater recharge. Simulations are continuous for 1000 yr of daily input and output, with soil water movement solved on smaller time steps as needed for numerical accuracy and convergence. However, the results can be interpreted as multiple realizations of shorter time series, each with a random, but physically realistic, initial condition for the first day of the starting year.

Energy and Carbon Balances

An important characteristic of WAVES is the coupling of water, energy, and carbon balances. Vertessy et al. (1996) summarized the use of solar energy and assimilation of carbon to drive dynamic plant growth and associated water use. Applying the integrated rate method (Hatton et al., 1992; Wu et al., 1994), plant growth is limited by the relative availabilities of light, water, and nutrients. Carbon assimilation and respiration from roots, stems, and leaves are included in an empirical representation of the vegetation response. This allows the leaf area to change dynamically with environmental conditions such as soil moisture, solar radiation, and atmospheric temperature. Thus, leaf area values need not be prespecified.

The energy balance is solved using the Penman–Monteith equation (after Monteith and Unsworth, 1990) to partition daily solar radiation provided by the climate simulator MWGEN. Solar radiation is attenuated by the canopy (only one layer is simulated here). Canopy resistances for heat and water vapor transfer are functions of the leaf area index, CO₂ concentration and air–mass vapor pressure deficit (vpd). Thus, evaporation is modeled explicitly for each climate.

Input Parameters

Input to the WAVES model includes climate variables for the two climate scenarios, soil hydraulic properties, and vegetation parameter sets. The same types of soils and vegetation are used at both sites for direct comparisons between climatic zones.

The daily climate variables simulated in MWGEN and used by WAVES are precipitation occurrence and amount, maximum and minimum temperature, and global solar radiation. In addition, WAVES requires vpd and computes vapor pressure inter-

nally. Monthly mean values of vpd were computed from humidity and temperature data at Cape Moreton near Stradbroke and at Pearce AFB for Gngangara (Bureau of Meteorology, 1988). These values were used in lieu of daily vapor pressure data for each climate scenario.

Soil parameters for four generic soil types (Table 1) cover the range of soils expected for relatively deep unsaturated soil profiles at Stradbroke and Gngangara, with most of the area composed of fine to medium sands (Ahmed et al., 1994).

Version 3.0a of WAVES uses a canopy-scale representation of the vegetation that appears to be robust under the various climatic conditions simulated here. The canopy-scale growth and decay are less dynamic (i.e., more conservative) than the leaf-scale dynamics simulated in previous versions (not shown here). We modified WAVES version 3.0a to include interday interception storage and enhanced user control of output for large simulation periods.

The plant-growth model uses parameters representative of eucalyptus or pine trees and perennial grasses tested under Australian conditions (Dawes and Zhang, 1998). Limited calibration periods, typically 2 or 3 yr, have been used to determine the sets of 17 vegetation parameters shown in Table 2, while simulations here are run for long time series assuming dynamic equilibrium in climate over decades to centuries.

Table 2 shows vegetation parameter sets for the four vegetation types: two perennial grasses (modified from the “WAVES Tutorial”; W. R. Dawes, personal communication, 1995) and two types of trees. Vegetation type Tree 1 is characterized by a balance of relatively high carbon assimilation rate (A_{\max}) and high leaf and root respiration [$R_{o(L,R)}$] and leaf mortality coefficients (m_L) after Vertessy et al. (1996), in contrast with Tree 2 (P.G. Slavich, personal communication). Nevertheless, leaf respiration coefficients are much higher for both grasses than for the trees. Also, Grass 1 and Tree 1 have the same relatively narrow temperature range for optimal growth. The maximum potential rooting depths vary between plant types (1.5 m for grasses and 10 or 15 m for trees), and actual rooting depths vary dynamically for each soil–plant–climate scenario. Although plants were allowed to respond dynamically to alterations in climate, plant types as designated by these parameter sets were fixed (the same for all climate scenarios).

An important assumption in this study is that the plant-growth model is able to simulate water use under climatic conditions that differ from those for which the model has been calibrated. We explicitly modified the model parameters that determine the changes in plant transpiration rates and vegetative cover due to CO₂ doubling (cf. Hatton et al., 1992). Two key parameters in our WAVES simulations were adjusted accordingly (Warrick Dawes, personal communication): the maximum carbon assimilation rate (A_{\max} in Table 2) was increased by 25%, and

TABLE 1. Soil hydraulic parameters (Broadbridge and White, 1988).†

| No. | Soil type | K_s m d ⁻¹ | θ_s | θ_o | λ_c m | C |
|-----|-------------|----------------------------|------------|------------|------------------|------|
| 1 | medium sand | 10.00 | 0.35 | 0.05 | 0.025 | 1.02 |
| 2 | fine sand | 1.00 | 0.35 | 0.08 | 0.05 | 1.02 |
| 3 | sandy loam | 0.20 | 0.40 | 0.07 | 0.10 | 1.15 |
| 4 | clay loam | 0.10 | 0.50 | 0.20 | 0.30 | 1.40 |

† K_s , saturated hydraulic conductivity; θ_s , saturated volumetric water content; θ_o , residual volumetric water content; λ_c , capillary length; C, fitting parameter.

a stomatal conductance parameter (g_1) was reduced by 50%. A similar approach was taken by Eckhardt et al. (2002), who modified the Soil Water Assessment Tool (Arnold et al., 1998).

Assessing Changes in Groundwater Recharge Regimes

The following methods were used to quantify changes in the simulated groundwater recharge time series. The measures below were applied to the differences in hydrologic response for each soil-vegetation combination at each study site. Climates 1 and 2 denote current and double CO₂ conditions, respectively, for a given location.

Measures of Long-Term Average Recharge

Two measures of the relative change in long-term average recharge highlight the net hydrologic response. The first measure, $Q_2/Q_1 = (\text{Recharge } 2)/(\text{Recharge } 1)$, is simply the net recharge under Climate 2 (double CO₂) normalized by the net recharge under Climate 1 (current conditions) for each soil–vegetation combination. Given a 14% increase in mean annual rainfall, for example, values greater than 1.14 indicate that, on average, a disproportionately high amount of rainfall in Climate 2 becomes recharge relative to the Climate 1 scenario. Values less than unity indicate a reduction in recharge, despite the increase in rainfall. The second measure is

$$\frac{\Delta Q}{\Delta R} = \frac{Q_2 - Q_1}{R_2 - R_1} \equiv \Delta(\text{Total recharge}) / \Delta(\text{Total rainfall}) \quad [2]$$

where Q_1 and Q_2 are the total drainage volumes (net recharge), and R_1 and R_2 are the total rainfall volumes under Climates 1 and 2, respectively. A value of zero would mean that, on average, all of the additional rainfall is transpired or evaporated (no additional recharge). A value of 1 means none of the additional

TABLE 2. Vegetation parameters for the WAVES model.

| Model parameter | | | Vegetation type | | | |
|---|--------------------------------------|-------------------|-----------------|---------|--------|--------|
| Description | Units | Symbol | Grass 1 | Grass 2 | Tree 1 | Tree 2 |
| Canopy albedo | – | α | 0.9 | 0.85 | 0.9 | 0.9 |
| Light extinction coefficient | – | χ_l | 0.65 | 0.65 | 0.42 | 0.40 |
| Maximum carbon assimilation rate | kg m ⁻² d ⁻¹ | A_{\max} | 0.0125 | 0.015 | 0.025 | 0.010 |
| Slope in stomatal conductance model | – | g_1 | 10. | 0.7 | 8.0 | 8.0 |
| Maximum plant available water potential | m | LWP_{\max} | 200. | 100. | 250. | 250. |
| IRM† weighting for light | – | w_h | 2.13 | 2.13 | 2.1 | 1.13 |
| IRM weighting for nutrients | – | w_n | 0.5 | 0.5 | 0.3 | 0.3 |
| Optimum temperature | °C | T_{opt} | 26 | 25 | 26 | 25 |
| Half optimal temperature | °C | T_{half} | 20 | 18 | 20 | 15 |
| Saturation light intensity | mmol m ⁻² d ⁻¹ | L_{\max} | 1200 | 1200 | 1000 | 1200 |
| Maximum rooting depth | m | RD_{\max} | 1.5 | 1.5 | 10. | 15. |
| Leaf respiration coefficient | kg kg ⁻¹ d ⁻¹ | R_{oL} | 0.003 | 0.003 | 0.0014 | 0.0008 |
| Root respiration coefficient | kg kg ⁻¹ d ⁻¹ | R_{oR} | 0.0004 | 0.0004 | 0.0008 | 0.0002 |
| Leaf mortality rate | kg kg ⁻¹ d ⁻¹ | m_L | 0.007 | 0.001 | 0.006 | 0.002 |
| Aerodynamic resistance | s m ⁻¹ | r_a | 50. | 50. | 20. | 20. |

† IRM, integrated rate methodology.

rainfall is transpired (on average, it all becomes recharge), and negative values indicate an even greater increase in evapotranspiration than in rainfall.

Temporal Persistence in Annual Recharge Variability

In addition to the statistics of mean annual recharge, water resource managers are concerned with interannual deficits or surpluses from a given demand. Here, we set the demand to the long-term average recharge, which equals the sustained yield including discharge to surface water bodies. Residual mass curves are used to quantify the temporal persistence of deviations for every soil–vegetation–climate combination. The residual mass is defined as

$$S_j = \sum_{i=1}^j (q_i - \bar{q}) \quad j = 1, \dots, n \quad [3]$$

where q_i is the recharge rate (mm yr^{-1}) in year i , \bar{q} is the average (net) recharge (mm yr^{-1}) after n years, and in this case, n is 1000 yr each aggregated from daily data. Instead of an actual mass, the units of S_j are given in millimeters as a sum of annual recharge deviations (mm yr^{-1}) over j years. The range in residual mass over a (long) time series has been used in computing a measure of the persistence in variations from the mean behavior. The Hurst coefficient H (Hurst, 1951; Salas, 1992) can indicate long-term dependence or persistence when $H > 0.5$ as estimated by

$$\hat{H} = \frac{\log(R_n/s_n)}{\log(n/2)} \quad [4]$$

where the range is

$$R_n = \max(S_j) - \min(S_j) \quad \forall j \leq n \quad [5]$$

and s_n is the sample standard deviation.

Another possible measure of persistence in annual recharge variability is the normalized range of residual mass:

$$P = R_n / \bar{q} = [\max(S_j) - \min(S_j)] / \bar{q} \quad \forall j \leq n \quad [6]$$

This persistence measure, P (P_1 and P_2 for Climates 1 and 2, respectively), is the ratio of a volume per unit area (mm) to an annual recharge rate (mm yr^{-1}), yielding units of time (yr). Both persistence measures H and P were computed for the simulated recharge below.

Results

Climate Generation

Climate scenarios are in the form of 1000 yr of generated daily weather data. Sample probability distributions for the daily meteorological variables are shown by season as box plots in Fig. 3. Climate variables are plotted separately for Stradbroke (Fig. 3a) and Gngangara (Fig. 3b). For each variable, double CO_2 conditions

(Climate 2) are plotted adjacent to (to the right of) present conditions (Climate 1) in panels separated by season. Seasons are defined in the figure caption. Extreme values in the tails of the distributions are plotted as horizontal lines beyond the whiskers at 1.5 times the interquartile ranges.

Simulated rainfall amounts [Fig. 3(i)] are highly skewed, and only nonzero values are plotted, with the sample size indicated above or beside each box plot. Box widths are also proportional to the square root of the number of rain days. These plots emphasize changes in extremes and the frequency of rainfall. Increases in the mean rainfall amount (37% at Stradbroke and 14% at Gngangara) are masked in this figure by the upper tails. The width of each box is proportional to the square root of the number of daily values, which varies only for daily rainfall amounts.

Alterations in the global solar radiation [Fig. 3(ii)] are relatively small and principally reflect changes in the number of rain days. The mean radiation decreased by 5.5% at Stradbroke

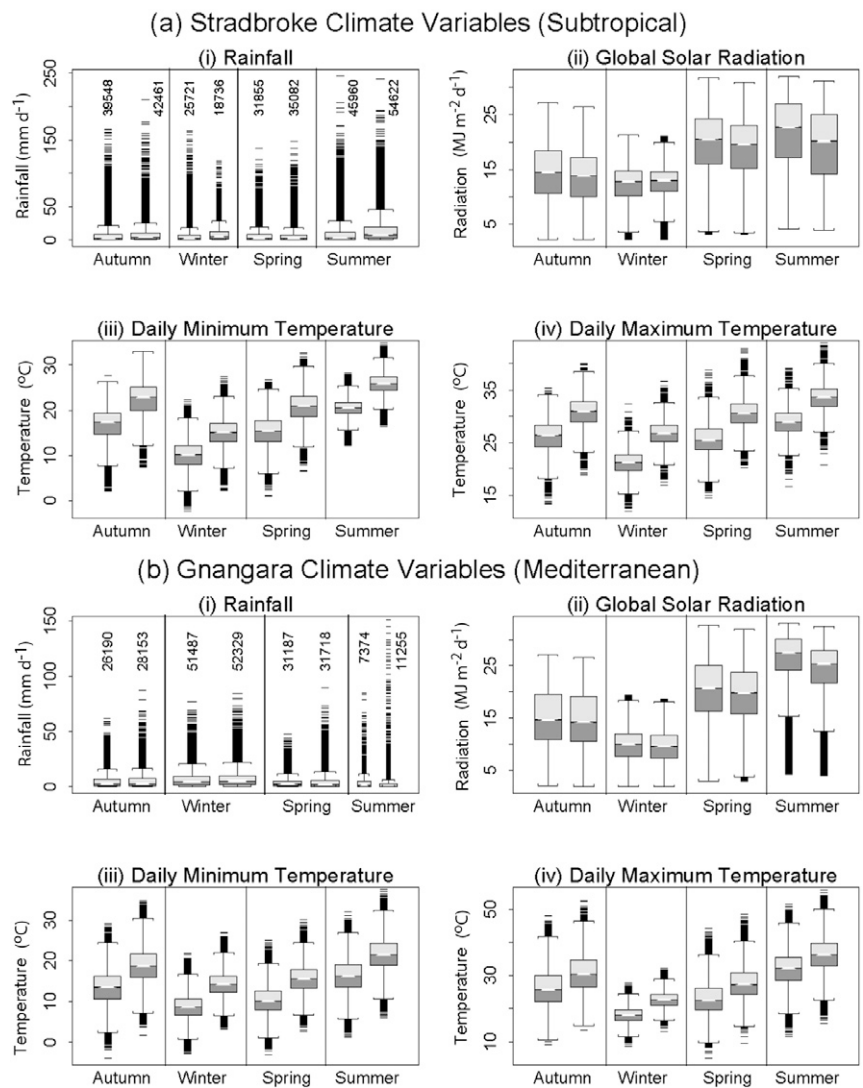


FIG. 3. Distributions of daily weather variables at (a) Stradbroke and (b) Gngangara with Climates 1 (present) and 2 (double CO_2) plotted side-by-side for: (i) rainfall amount (ii) global solar radiation, (iii) minimum temperature, and (iv) maximum temperature. The total number of rainfall events is shown with each rainfall box plot. Boxes show 25, 50 (median), and 75% quartiles, and whiskers span 1.5 times the interquartile ranges or to the most extreme (maximum or minimum) value; “extreme values” beyond the whiskers are plotted as horizontal lines.

and 5.2% at Gngangara, while the seasonal ranges were relatively unchanged in both locations. Simulated changes in daily minimum [Fig. 3(iii)] and maximum [Fig. 3(iv)] temperatures are approximately 5°C for the median values, and the spread (variance and skewness) is similar for both climates. The average daily minimum temperature increased more than the maximum ($\Delta T_{\min} = 5.3^\circ\text{C}$ and $\Delta T_{\max} = 5.0^\circ\text{C}$ for Stradbroke, and $\Delta T_{\min} = 5.3^\circ\text{C}$ and $\Delta T_{\max} = 4.9^\circ\text{C}$ for Gngangara).

The resulting histograms of wet- and dry-period durations at Stradbroke are shown in Fig. 4. The semi-log scale emphasizes the projected increase of long-duration periods of both continuous rain (wet) days and no rain (dry). A frequency of 1 would be zero on the log scale, so a small positive value was added for plotting purposes. Wet-period durations of more than 6 d and dry-period durations of more than 20 d were more frequent for double CO₂ conditions (Climate 2) than for present conditions (Climate 1). The maximum wet- and dry-period durations for these sample distributions increased from 40 to 56 d and 87 to 109 d, respectively. Changes in the wet- and dry-period durations at Gngangara (not shown) were less pronounced.

Recharge Simulations

Example Time Series for Stradbroke

Simulated evapotranspiration and the resulting long-term average value of groundwater recharge (“drainage” below the root zone) changed disproportionately with rainfall. The net recharge can more than double with an increase in mean annual rainfall from 1.13 to 1.56 m (37%) and a mild increase in the average number of wet days (from 39 to 41%). This result is related primarily to the increased frequency of long-duration wet and dry periods (Fig. 4). Figure 5 shows a 10-yr window of monthly aggregated rainfall, plant growth, and hydrologic responses during a period containing the longest simulated dry period for both climate scenarios. Only one simulated vegetation type (Tree 1) is shown for illustration. During long dry spells, plants senesce, reducing their leaf area and root density. This decreases the transpiration from subsequent infiltration events compared with that of healthy plants experiencing similar water availability. Thus, more water is allowed to drain beyond the root zone. Longer wet periods and increased daily rainfall amounts also enhance the recharge volume and peak drainage rates.

The nonlinear responses of mean recharge to mean rainfall are due to simulated reductions in the mean evapotranspiration (ET) under the simulated climate change. Simulated values of ET are reasonable (fluctuating around approximately 2 mm day⁻¹ for Climate 1 in the period shown in Fig. 5 for Stradbroke), but independent estimates of actual ET from historical data are not available for direct comparison. In WAVES ET is partitioned between plant transpiration and evaporation from soil and rainfall interception by the canopy. Thus, simulated changes in leaf area affect all components of the total ET.

Daily recharge rates vary much more gradually than the intermittent rainfall that drives the unsaturated flow system. This dampening of the drainage response at depth is caused by the flow impedance and storage capacity of the vadose zone and thus depends on the depth at which deep drainage (i.e., water that will become groundwater recharge at the water table) is

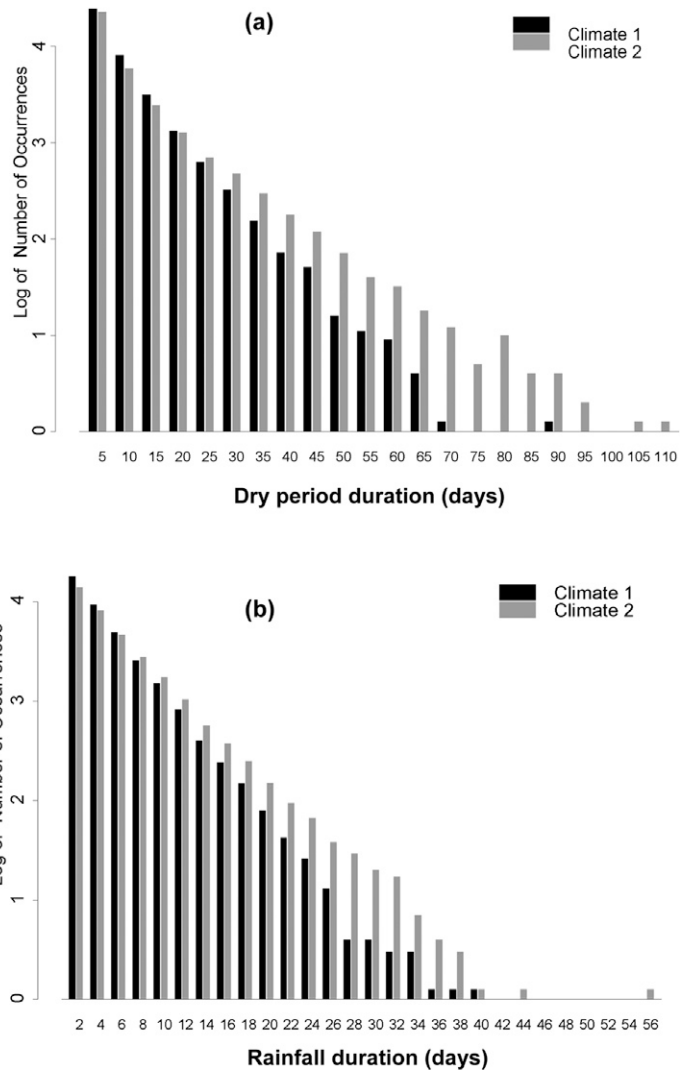


Fig. 4. Frequency histograms of (a) dry-period durations and (b) wet-period durations for Stradbroke only. Climates 1 and 2 are current and double CO₂ conditions, respectively. Bars are plotted on a log₁₀ scale, and single-occurrence events [$\log_{10}(1) = 0$] are plotted as 0.1 instead of 0 for graphical purposes to show the extremes.

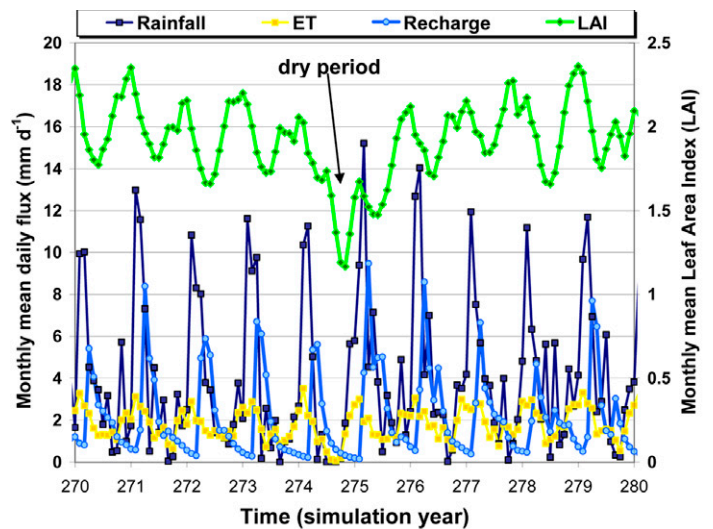


Fig. 5. Example time series (monthly aggregates) of input flux: Rainfall; output fluxes: evapotranspiration (ET) and recharge; and leaf area index (LAI) for a 10-yr window including the longest dry period simulated at Stradbroke for the double CO₂ scenario with fine sand (Table 1) and Grass 1 (Table 2).

simulated. That depth was 5 m for the grasses and 25 m for the trees.

Annual Recharge Distributions

An annual timescale is appropriate for assessment of groundwater recharge, keeping in mind that temporal dynamics of the recharge to the water table will differ somewhat from the simulated gravity drainage at 5 or 25 m for grasses and trees, respectively. The following analyses used annual aggregates of the simulated daily drainage (“recharge”).

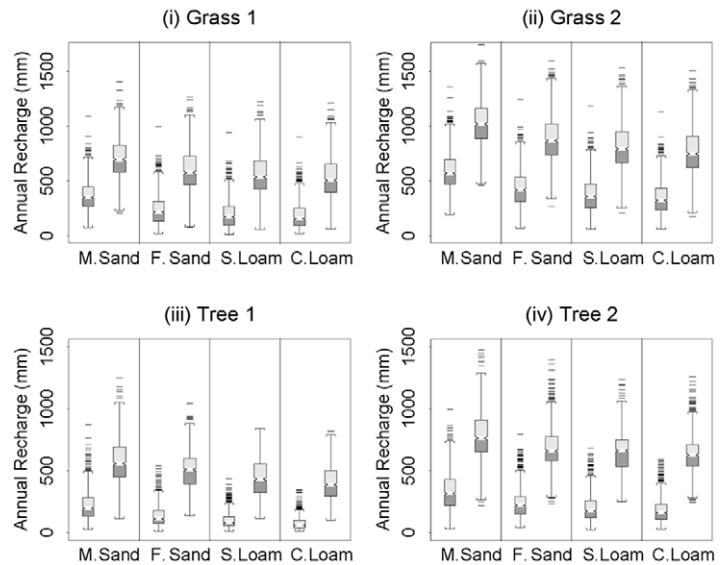
Box Plots

Figure 6a shows box plots of 1000 annual recharge values for each combination of vegetation and soil types at Stradbroke. Climates 1 and 2 are plotted side-by-side in each soil-type panel to illustrate the changes in median annual recharge. (The notches indicate 95% confidence intervals for the medians, showing that the changes in median values are generally significant at that level.) For each climate and with every type of vegetation, the median annual recharge decreased with finer soil texture. This is due to increased water availability in the root zone as percolating water is held more strongly by capillarity in the finer textured soils. Also, the temporal variance tends to decrease with finer soil texture due to increased transit times and diffusion of wetting fronts. Grass 1 allowed less recharge than Grass 2 under both climate scenarios at Stradbroke. This may be due to a combination of a lower stomatal conductance associated with g_1 (see Table 2; $g_1 = 10$ for Grass 1 and $g_1 = 0.7$ for Grass 2) and the maximum plant available water potential for Grass 2 being half that of Grass 1 (Table 2).

The general pattern of increased temporal variation under Climate 2 may be related to both the increased average annual rainfall amount (“climate change”) and to the variations in rainfall occurrence and associated duration frequencies (“climate variability”). Climate change may increase the average water content of the soil profile, which decreases the system response time, particularly for high recharge events. Climate variability affects within-year wetness patterns, particularly following dry spells or long periods of consecutive rain days; this has a non-linear effect on vertical water flow and extraction by roots, as well as dynamic vegetative cover and associated transpiration demands. Such dynamic model responses are shown in Fig. 5, where in simulation year 275, low rainfall resulted in reduced evapotranspiration and deep drainage (recharge), but the associated reduction in leaf area allowed subsequent drainage to increase rapidly.

Figure 6b shows box plots of 1000 annual recharge values for each combination of vegetation and soil type at Gngangara. For each canopy (vegetation type), the direction of change in recharge was the same for all four soil types. Unlike Stradbroke, however, both the magnitude and the direction of change differed among vegetation types. Recharge was reduced beneath some canopies (Grass 1 and Tree 1) despite the increase in mean rainfall. A pronounced difference between grasses and trees in the annual recharge amounts was simulated at Gngangara (Fig. 6b), particularly for fine-textured soils. This is consistent with documented effects of tree clearing on increased groundwater recharge (Peck and Williamson, 1987) and associated increases in soil salinity (Williamson et al., 1987). As shown in Table 2,

(a) Stradbroke: Simulated Annual Recharge



(b) Gngangara: Simulated Annual Recharge

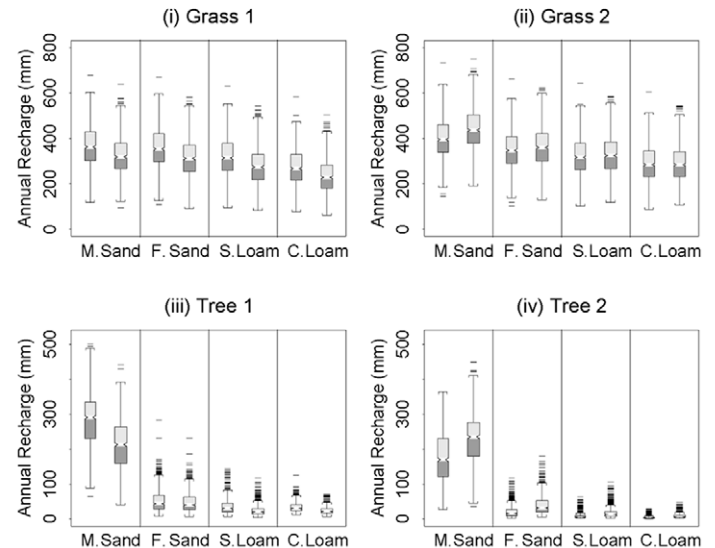


FIG. 6. Box plots of annual recharge amounts for 1000 yr of simulation showing current and double CO_2 conditions side-by-side in panels for each soil type (medium sand, fine sand, sandy loam, clay loam). Climate scenarios are shown for (a) Stradbroke and (b) Gngangara. Vegetation types are indicated for each subplot (i)–(iv). Whiskers span 1.5 times the interquartile ranges or to the most extreme (maximum or minimum) value, and “extreme values” beyond 1.5 whiskers are plotted as horizontal lines.

the primary differences between grasses and trees are quantified by the light extinction coefficient; IRM (integrated rate methodology), weighting for light; maximum potential rooting depth; leaf respiration coefficient; and aerodynamic resistance. Although simulated recharge may be sensitive to other vegetation parameters, such as the maximum carbon assimilation rate and optimum temperature, these parameters differ among grasses or trees as much as between grasses and trees. The present results show interesting sensitivities to vegetation parameters, but a detailed sensitivity analysis is left for further research.

The net recharge can more than double with an increase in mean annual rainfall from 642 to 732 mm (14%) and a mild increase (2%) in the average number of wet days (from 116 to 123). This result is related primarily to the increased frequency of long-duration wet periods and to the change in growth rates associated with changes in the temperature regime. Increased temperatures account for the simulated reductions in recharge with increased rainfall. The effects of such interactions could not be predicted a priori and thus demonstrate the utility of the present simulation approach including the effects of dynamic plant growth and water use.

Again, the median annual recharge for each climate scenario decreased with finer soil texture for all vegetation types. We also note the pronounced effect of soil texture on recharge beneath tree canopies for either climate scenario at Gngangara versus milder effects in the same direction at Stradbroke. This may be because of higher rainfall amounts at Stradbroke and the seasonal nature of rainfall in these different climatic zones. Within an average year, rainfall is more uniform in the subtropical climate at Stradbroke than in the Mediterranean climate at Gngangara. More winter rainfall at Gngangara escapes the root zone in the medium (or coarser) sand but is held for transpiration later in the year by finer-textured soils. It is not entirely clear, however, why grasses are not affected in a similar way, except to postulate that similar amounts of infiltrated rainfall escape their relatively shallow root zones within the wet season for all soil types.

Quantile–Quantile Plots

A direct comparison of the change in annual recharge between climate scenarios is possible using quantile–quantile (q–q) plots. If there were no change in temporal distributions of recharge, points would fall on a 1:1 line. If alterations in the recharge regimes were proportional to alterations in rainfall, all points (quantiles) would fall along a straight line passing through the origin. Figure 7 shows q–q plots for each combination of vegetation (rows) versus soil (columns), with Climate 1 on the horizontal axes and Climate 2 on the vertical axes. Dashed lines mark the 1:1 equality, and solid lines are linear regressions to the simulated data. Above each q–q plot are two numbers stating the intercept and slope of the regression line.

For Stradbroke (Fig. 7a) the offsets (intercepts) are significant, ranging from 22 to 36 cm yr^{-1} , and the slopes are consistently greater than unity, ranging from 1.18 to 2.41. The q–q plots tend to be nonlinear, and the lower tails turn toward the 1:1 line at the origin to some degree in every case. This deviation from the offset line can be explained by low recharge scenarios under the current climate remaining relatively low under double CO_2 conditions. In general, the annual recharge patterns are altered substantially by the climate alteration (note changes in rainfall frequency-duration and dry-period duration in Fig. 4).

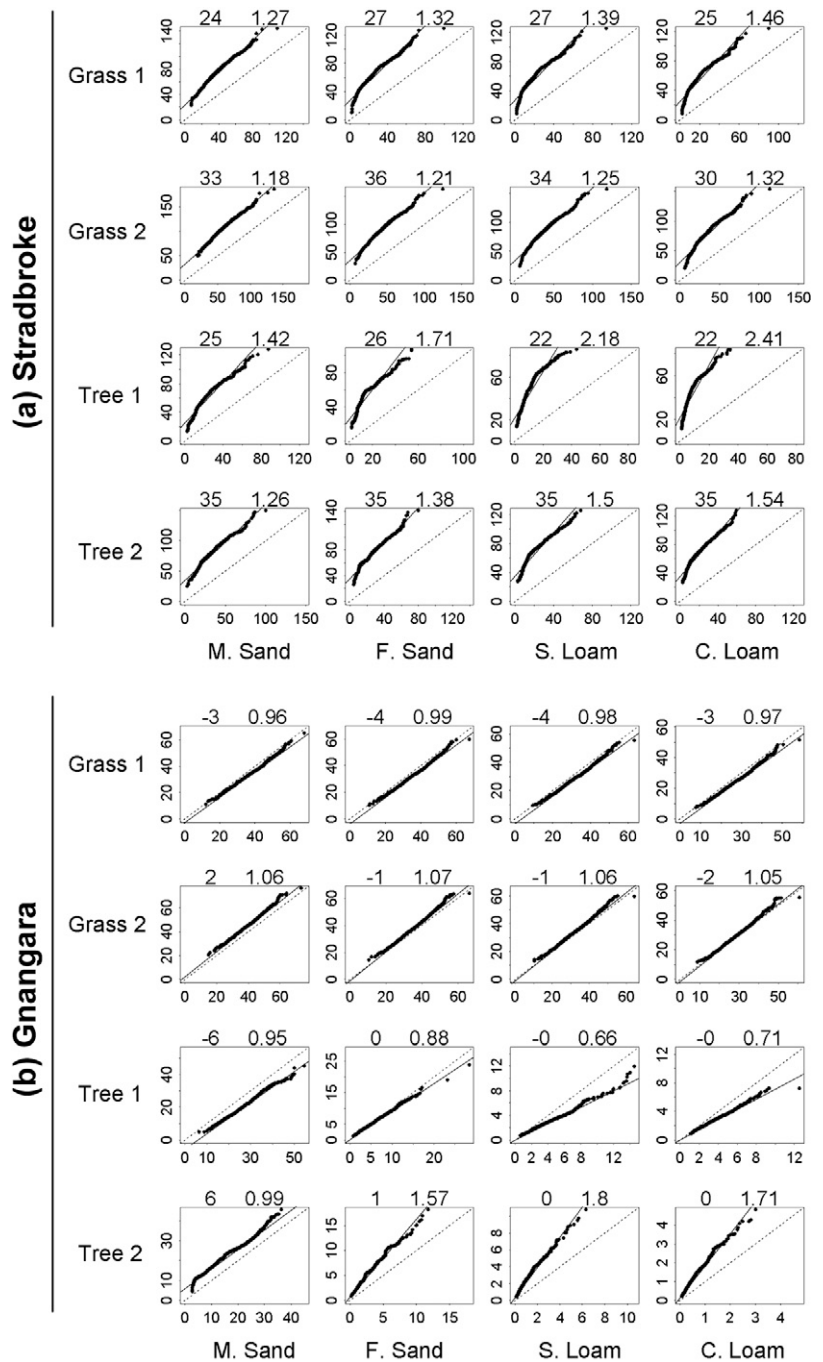


FIG. 7. Quantile–quantile plots of annual recharge amounts for 1000 yr of simulation showing double CO_2 vs. current conditions for each soil type (columns) and vegetation type (rows). Climate scenarios are shown for (a) Stradbroke and (b) Gngangara. Numbers above each plot are the intercept and slope of the regression (solid) line. The dotted line has an intercept of 0 and slope of 1. Units of recharge are cm yr^{-1} on both axes. (M = medium, F = fine, S = sandy, C = clay.)

For Gngangara (Fig. 7b) the changes in recharge are generally much less pronounced. This is particularly true for the grasses, where the points lie close to the 1:1 line. The most dramatic effects occur beneath the tree canopies. The intercepts are generally near zero, and the slopes range from 0.66 to 1.80. Interestingly, these extremes are observed on the same soil type (sandy loam) with different tree types. Although the soils affected the absolute value of recharge for each climate scenario (see Fig. 6b), the ratio of change in recharge may have been affected more

by the vegetation type. The consistent decreases for both Grass 1 and Tree 1 appear to be related to their relatively narrow range of optimal temperature (see Table 2) and corresponding shifts in temperature into the peak zone for Climate 2. Finally, changes in the recharge regimes tend to be more linear for Gngangara than for Stradbroke.

Long-Term Mean Recharge

Measure 1

Figure 8 shows results using the first measure of long-term net change, Q_2/Q_1 , for various combinations of four soil types and four types of vegetation at both locations. At Stradbroke (Fig. 8a) Q_2/Q_1 ranges from 1.74 to 5.09, consistently increasing in value from coarse to finer textured soils and from Tree 2 (row 4) up to Grass 1 (row 1). There was an increase in sensitivity to climate alteration going from trees to grass, as well as a consistent increase from vegetation with moderate assimilation and respiration rates to those with a balance of relatively high rates. The latter balance yields greater temporal variation in plant biomass, including leaf area. That is, more dynamic plants are more susceptible to extended wet and dry periods (climate variability) associated with the climate change scenario. At Gngangara (Fig. 8b) Q_2/Q_1 ranges from 0.66 for Tree 1 to 2.19 for Tree 2 (both values occurring with sandy loam, soil type 3). The trees experienced the greatest changes in recharge with climate, while the effect was less pronounced with grasses.

Measure 2

Figure 9 shows the results in terms of $\Delta Q/\Delta R$ (Measure 2, given in Eq. [2]). For Stradbroke (Fig. 9a) there was no trend with soil type, and the principal changes ($\Delta Q/\Delta R$ ranging from 0.76 to 1.05) were related to vegetation. The alternating bands of dark and light indicate that it is not a distinction between grasses and trees. Rather, it appears to relate to the magnitude of carbon assimilation and plant respiration (see Table 2), and the associated dynamics of leaf area and plant available radiation. For Gngangara (Fig. 9b), the principal differences (in a range of -0.79 to 0.62) were related to vegetation also. The alternating bands of dark and light (most pronounced for the medium sand, soil type 1) again indicate that it is not a distinction between grasses and trees. Rather, it relates to the temperature ranges for optimal growth (see Table 2) and the associated dynamics of leaf area and plant available radiation. This sensitivity decreased for the finer textured soils, and most of the recharge beneath trees occurred in the coarser soils.

The effects of dynamic versus static vegetation were tested on the trees by rerunning the model for Stradbroke with a constant leaf area index, and with root and stem carbon set to average values of the dynamic time series. These runs were limited to 100 yr, which was sufficient for testing differences in mean recharge rates. Values of $\Delta Q/\Delta R$ decreased consistently by approximately 0.1, indicating that vegetation dynamics are responsible for making $\Delta Q/\Delta R$ exceed 1.0, but other factors affect the first-order difference in recharge between vegetation types. The comparison between dynamic and static vegetation is not illustrated here.

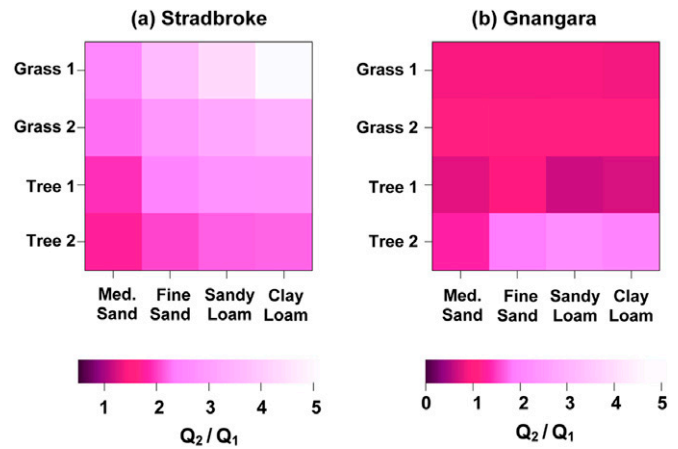


FIG. 8. Ratio (Measure 1) of net recharge for double CO_2 (Q_2) divided by current CO_2 conditions (Q_1) vs. soil and vegetation type for (a) subtropical Stradbroke and (b) Mediterranean Gngangara.

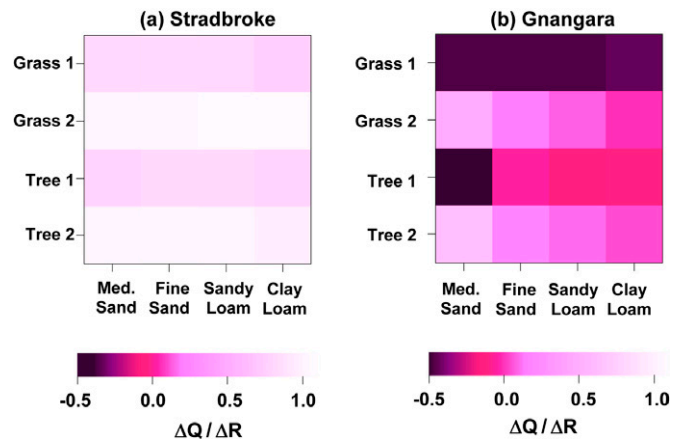


FIG. 9. Ratios of the change in net recharge to change in total rainfall (Measure 2, Eq. [2]) vs. vegetation and soil type for (a) subtropical Stradbroke and (b) Mediterranean Gngangara.

Temporal Persistence in Annual Recharge Variability

We computed estimates of \hat{H} for each soil–vegetation–climate scenario as described above. For Stradbroke Climates 1 and 2, values fell in the ranges $0.585 < \hat{H} < 0.713$ and $0.546 < \hat{H} < 0.614$, respectively. For Gngangara Climates 1 and 2, values fell in the ranges $0.556 < \hat{H} < 0.713$ and $0.566 < \hat{H} < 0.733$, respectively. Although these ranges have large overlaps, and we do not connote statistical significance here, the value of \hat{H} for given soil–vegetation environments generally decreased at Stradbroke while increasing at Gngangara. An increase in \hat{H} indicates an increase in the persistence of deviation from the mean recharge, regardless of the direction of change in the mean. Example plots of the residual mass for each climate at Stradbroke are shown for Tree 2 and fine sand in Fig. 10. These plots include annual recharge rates, a 10-yr running average, cumulative running average (Net) recharge, and the annual residual mass curve. Because the number of years simulated is the same for all scenarios ($n = 1000$), the computed Hurst coefficient \hat{H} is based on the ratio of the range in residual mass R_n divided by the standard deviation of annual recharge s_n simulated for each scenario. In Fig. 10 the range R_n changed from approximately 5800 to 7500 mm for Climates 1 and 2, respectively, but \hat{H} decreased slightly due to the associated increase in s_n for the scenarios shown. Thus, the

Hurst coefficient can reflect a change in temporal persistence which is not captured by the change in variance alone.

The persistence measure, P (P_1 and P_2 for Climates 1 and 2, respectively), is the ratio of a volume per unit area (mm) to an annual recharge rate (mm yr⁻¹), yielding units of time (yr). Unlike H , P is not normalized by the length of record n , so the absolute value of P is a function of n , where n is 1000 for all scenarios simulated here. The variation in P_1 with vegetation and soil types is shown in Fig. 11a and 11b. For Stradbroke Climate 1, the range is $11 < P_1 < 67$ yr. In contrast, for Stradbroke Climate 2, the range is much smaller: $6 < P_2 < 14$ yr (not shown graphically). The average persistence for Stradbroke Climate 2 is much less than that for Stradbroke Climate 1, despite the increased variance in annual recharge under double CO₂ conditions. For Gngangara Climate 1, the range is $7.1 < P_1 < 84$ yr, while, for Gngangara Climate 2, the range decreased slightly to $7.0 < P_2 < 74$ yr.

Figures 11c and 11d show the resulting ratios of P_2 to P_1 , ranging from 0.24 to 0.57 at Stradbroke and from 0.79 to 1.35 at Gngangara. Two possible factors are contributing to the differences in persistence of recharge between the two climates. First, R_n is normalized by the mean recharge, which can be significantly greater for Climate 2, thus compensating for the somewhat greater ranges in residual mass. Second, the same physical mechanism (i.e., increased water contents in the soil profile) that caused the variance in annual recharge to increase also decreased the persistence of such deviations from the mean at Stradbroke, where mean rainfall was increased by 37%. There is a nonlinear increase in unsaturated hydraulic conductivity and decrease in soil-moisture deficit with increased water content; these factors can reduce the system response time and associated temporal persistence. At Gngangara the range spanning unity reflects the changes in simulated recharge both increasing and decreasing with climate change, despite the 14% increase in mean rainfall. Ultimately, the simulated changes in temporal persistence indicated above are caused by both the temporal correlation structures of the climate variables, particularly daily rainfall simulated with MWGEN, and the water and vegetation dynamics simulated with WAVES.

General Discussion and Caveats

The methods developed and applied here provide a quantitative guide to the direction of change and the potential significance of changes in evapotranspiration, soil moisture, and groundwater recharge regimes due to simulated climate change. As with any numerical experiment, the results are only indicative of the potential responses of real-world systems. There are a number of important qualifications to this assessment of the effects of climate alteration on groundwater resources:

- Climate scenarios derived from one GCM are uncertain based on the present disagreement among GCMs. A complete study of climate change impacts would include the use of results from several GCMs (Watson et al., 1996). Nevertheless, climate change scenarios produced by CSIRO9 were shown to fall within

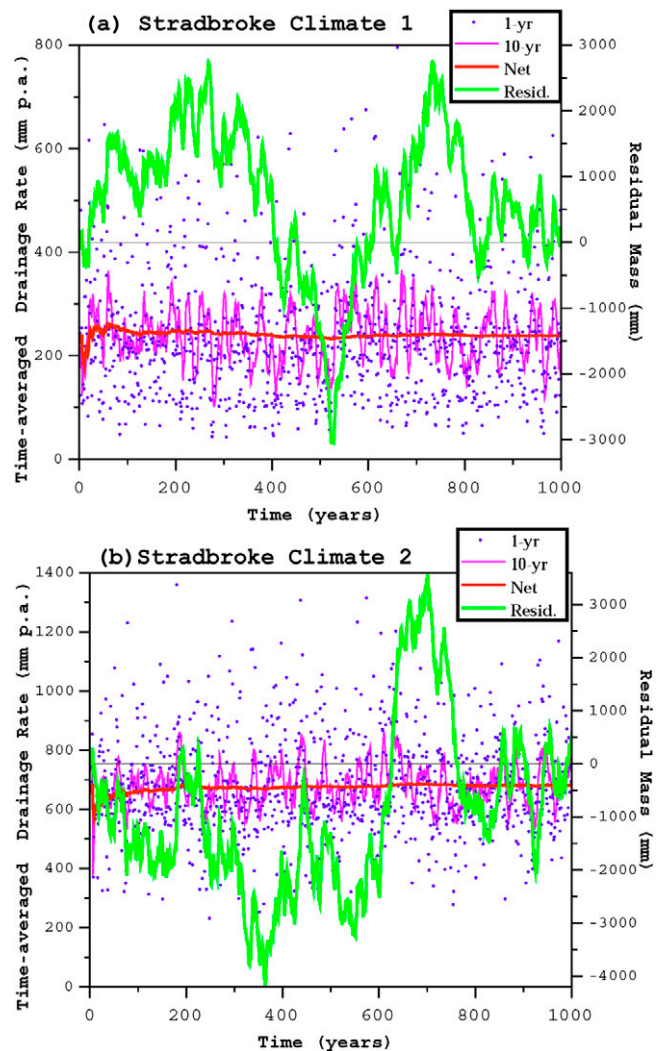


FIG. 10. Example plots of annual recharge (dots), 10-yr running average (10-yr), long-term running average (Net), and residual mass curve (Resid.) for 1000 yr of simulation time using Tree 2 in fine sand for (a) current CO₂ and (b) double CO₂ conditions at Stradbroke.

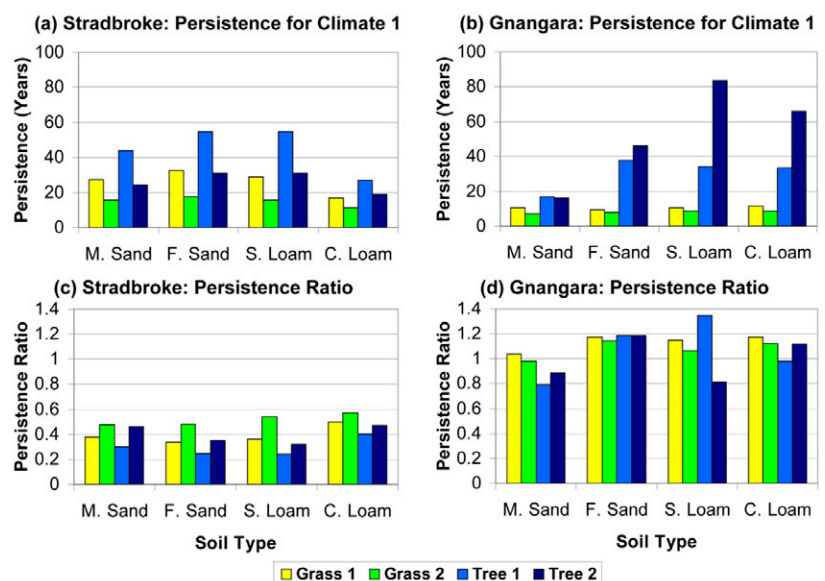


FIG. 11. Persistence measure (Eq. [6]) for Climate 1 (P_1) vs. vegetation and soil type at (a) Stradbroke and (b) Gngangara, and ratios of this persistence measure for Climate 2 divided by Climate 1 (P_2/P_1) at (c) Stradbroke and (d) Gngangara. (M = medium, F = fine, S = sandy, C = clay.)

the range of conditions simulated by other models (Chen et al., 1997).

- As noted by Whetton et al. (1996), the present generation of GCMs do not explicitly simulate the El Niño–Southern Oscillation (ENSO), tropical cyclones, rain depressions, or extra-tropical lows, and cold fronts. These are the main sources of widespread heavy rain at Stradbroke and are the major sources of groundwater recharge events for that climate (Fleming, 1995).
- An important assumption in this study is that the plant-growth model is able to simulate water use under climatic conditions that differ from those for which the model has been calibrated. Despite this potential limitation, possible changes in plant transpiration rates and vegetative cover have been considered by including the effects of CO₂ doubling on (increased) carbon assimilation and (decreased) stomatal conductance.
- Although biomass (above and below ground) is simulated dynamically, vegetation types are assumed to be the same for both climates. It is likely that plant communities would adapt in terms of physiological response and species composition under CO₂-altered climates. This phenomenon of coupling plant communities to climate alteration is beyond the scope of the present paper.

Summary and Conclusions

The simulated effects of CO₂-altered climates on groundwater recharge were related directly to the local soil–water–vegetation system. The direction and magnitude of the change in local recharge depended on the combination of climate scenarios, vegetation, and soil properties. It is not possible to make generic conclusions about climate change impacts based on this limited sample of climatic zones in Australia. Thus, we emphasize the development and demonstration of methods for the assessment of climate change impacts and potential sensitivities to particular climate variables and their temporal regimes. New aspects of this study include the method for generating climate sequences, simulation of vegetation growth and dynamics in response to current and double CO₂ climate sequences, and application to two different climatic zones (subtropical and Mediterranean) with summer- and winter-dominated rainfall regimes, respectively.

For the Stradbroke (subtropical) climate scenarios, simulated net recharge consistently increased by amounts approaching, and in some cases greater than, the change in total rainfall. Vegetation type affected the transpiration and resulting recharge more than soil type, but both played important roles. The present simulations indicated that recharge can more than double (Q_2/Q_1 ranging from 1.74 to 5.09) under the projected climate change of a mean annual increase in rainfall amount of 37% ($R_2/R_1 = 1.37$). These results for a subtropical climate change scenario in Australia differ from the relative insensitivity of groundwater recharge to a climate change scenario in central Europe (Eckhardt and Ulbrich, 2003). Our greatest changes in recharge occurred with perennial grasses, which may be more susceptible to the impacts of climate alteration than eucalyptus trees in subtropical climates.

For the Gngangara (Mediterranean) climate scenarios, soil texture played an important role for the trees but had a less

dramatic effect for grasses. The simulations indicated that the recharge can either decrease or more than double (Q_2/Q_1 ranging from 0.66 to 2.19) under the projected climate change, with a mean annual increase in rainfall amount of 14% ($R_2/R_1 = 1.14$). Unlike simulations for subtropical climate scenarios at Stradbroke, the results for the Mediterranean climate scenarios at Gngangara did not show a consistent increase in recharge for all vegetation types. These results appear to be controlled primarily by the optimal temperature range for plant growth, rather than by maximum carbon assimilation and respiration rates or changes in dry period durations. The feasibility of these results appears to be confirmed by recent WAVES simulations at Gngangara (Wanneroo Station) where *Pinus pinaster* plantations can transpire additional sources of water beyond the annual average rainfall of 750 mm yr⁻¹ (Warrick Dawes, personal communication).

Changes in the long-term net recharge (i.e., sustainable aquifer discharge to natural and manmade systems) and the interannual variation in recharge were shown for various soil–vegetation combinations (Fig. 6). Increases in recharge variability and decreases in persistence of deviations from the mean annual recharge (or vice versa) were related to the general change in average system wetness and nonlinear response of the soil–water system. The subtropical climate change resulted in consistent decreases in the temporal persistence of recharge associated with increased mean recharge and soil water content.

The simulation results presented here are indicative of substantial changes in recharge regimes in the moderately deep, unconfined portions of the aquifers underlying North Stradbroke Island and the Gngangara region due to climate change. More detailed estimates of the potential changes in spatially averaged recharge would be possible, given knowledge of the cross-correlated spatial distributions of soil and vegetation types from more detailed site data. Shallow water table conditions could also be simulated using WAVES for such assessments. In concert with the methods demonstrated here, improved understanding and simulation of plant growth and transpiration responses are essential for reducing the uncertainty of estimates of the effects of climate change and climate variability on groundwater resources.

References

- Ahmed, M., M.L. Sharma, Q.D. Richards, and A.R. Ahmad. 1994. Field-scale nitrogen leaching: Application of model 'LEACHN'. p. 45–54. *In* B.Y. Aminuddin, M.L. Sharma, and I.R. Willett (ed.) *Agricultural impacts on groundwater quality*. ACIAR Proceedings 61. ACIAR, Canberra, Australia.
- Alley, W.M., R.W. Healey, J.W. LaBaugh, and T.E. Reilly. 2002. Flow and storage in groundwater systems. *Science* 296:1985–1990.
- Arnold, J.G., R. Srinivasan, R.S. Muttiah, and J.R. Williams. 1998. Large area hydrologic modelling and assessment, part I: Model development. *J. Am. Water Resour. Assoc.* 34:73–89.
- Bajjali, W., and N. Abu-Jaber. 2001. Climatological signals of the paleogroundwater in Jordan. *J. Hydrol.* 243:133–147.
- Bates, B.C., S.P. Charles, N.R. Sumner, and P.M. Fleming. 1994. Climate change and its hydrological implications for South Australia. *Trans. R. Soc. South Aust.* 118:35–43.
- Bell, V.A., A.L. Kay, R.G. Jones, and R.J. Moore. 2007. Development of a high resolution grid-based river flow model for use with regional climate model output. *Hydrol. Earth Syst. Sci.* 11:532–549.
- Broadbridge, P., and I. White. 1988. Constant rate rainfall infiltration: A versatile nonlinear model: 1. Analytic solution. *Water Resour. Res.* 24:145–154.
- Brutsaert, W.F. 1971. A functional iteration technique for solving the Richards

- equation applied to two-dimensional infiltration problems. *Water Resour. Res.* 7:1583–1596.
- Bureau of Meteorology. 1988. Climatic averages, Australia, meteorology summary, July 1988. Bureau of Meteorology, Government of Australia.
- Chen, T.H., A. Henderson-Sellers, P.C.D. Milly, et al. 1997. Cabauw experimental results from the project for intercomparison of land-surface parameterization schemes. *J. Clim.* 10:1194–1215.
- CSIRO. 1992. Climate change scenarios for the Australian region. Available at http://www.cmar.csiro.au/e-print/open/CIG_1992a.pdf (verified 4 May 2007). CSIRO Division of Atmospheric Research, Aspendale, VIC, Australia.
- CSIRO. 1996. 1996 climate change scenarios. Available at <http://www.cmar.csiro.au/e-print/open/scenarios.htm> (verified 4 May 2007). CSIRO Division of Atmospheric Research, Aspendale, VIC, Australia.
- CSIRO. 2001. Climate change projections for Australia. Available at <http://www.cmar.csiro.au/e-print/open/projections2001.pdf> (verified 4 May 2007). CSIRO Division of Atmospheric Research, Aspendale, VIC, Australia.
- Dawes, W.R., and D.L. Short. 1993. The efficient numerical solution of differential equations for coupled water and solute dynamics: The WAVES model. 93/18, CSIRO Division of Water Resources, Canberra, Australia.
- Dawes, W.R., and L. Zhang. 1998. WAVES: An integrated energy and water balance model. Available at <http://www.clw.csiro.au/products/waves/> (verified 1 May 2007). CSIRO, Clayton South, VIC, Australia.
- Dooge, J.C.I. 1992. Hydrologic models and climate change. *J. Geophys. Res.* 97(D3):2677–2686.
- Eckhardt, K., S. Haverkamp, N. Fohrer, and H.-G. Frede. 2002. SWAT-G, a version of SWAT99.2 modified for application to low mountain range catchments. *Phys. Chem. Earth* 27:641–644.
- Eckhardt, K., and U. Ulbrich. 2003. Potential impacts of climate change on groundwater recharge and streamflow in a central European low mountain range. *J. Hydrol.* 284:244–252.
- Farrington, P., G.D. Watson, G.A. Bartle, and E.A.N. Greenwood. 1990. Evaporation from dampland vegetation on a groundwater mound. *J. Hydrol.* 115:65–75.
- Fleming, P.M. 1987. The role of radiation estimation in the areal water balance in tropical regions: A review. *Arch. Hydrobiol. Beih.* 28:19–27.
- Fleming, P.M. 1995. Australian water resources are different. *Australasian Sci.* 16:8–10.
- Green, T.R., B.C. Bates, P.M. Fleming, and S.P. Charles. 1997. Simulated impacts of climate change on groundwater recharge in the subtropics of Queensland, Australia. p. 187–204. *In* M. Taniguchi (ed.) *Subsurface hydrological responses to land cover and land use changes*. Kluwer Academic, Boston, MA.
- Hatton, T.J., J. Walker, W. Dawes, and F.X. Dunin. 1992. Simulations of hydroecological responses to elevated CO₂ at the catchment scale. *Aust. J. Bot.* 40:679–696.
- Hennessy, K.J., I. Macadam, and P.H. Whetton. 2006. Climate change scenarios for initial assessment of risk in accordance with risk management guidance. Available at <http://www.greenhouse.gov.au/impacts/publications/pubs/risk-scenarios.pdf> (verified 1 May 2007). CSIRO Marine and Atmospheric Research, Aspendale, VIC, Australia.
- Hennessy, K.J., and P.H. Whetton. 2001. Comparison of CSIRO climate change scenarios released in 1996 and 2001. Available at <http://www.dar.csiro.au/impacts/docs/comparison.pdf> (verified 1 May 2007). Climate Impact Group, CSIRO Division of Atmospheric Research, Aspendale, VIC, Australia.
- Holper, P. 2002. The greenhouse effect. Available at http://www.cmar.csiro.au/e-print/open/holper_2001b.html (verified 2 May 2007). CSIRO Division of Atmospheric Research, Aspendale, VIC, Australia.
- Hurst, H.E. 1951. Long term capacities of reservoirs. *Trans. Am. Soc. Civ. Eng.* 116:776–808.
- Knight, J.H., and J.R. Philip. 1979. Exact solutions in nonlinear diffusion. *J. Eng. Math.* 8:219–227.
- Laycock, J.W. 1975. North Stradbroke Island: Hydrogeological report. Rep. no. 88. Geological Survey of Queensland, Brisbane, Australia.
- Loáiciga, H.A., D.R. Maidment, and J.B. Valdes. 2000. Climate-change impacts in a regional karst aquifer, Texas, USA. *J. Hydrol.* 227:173–194.
- McCarthy, J.J., O.F. Canziani, N.A. Leary, D.J. Dokken, and K.S. White. 2001. Climate change 2001, impacts, adaptation, and vulnerability. Contribution of Working Group II to the Third Assessment Report of the IPCC. Available at http://www.grida.no/climate/ipcc_tar/wg2/index.htm (verified 1 May 2007). Intergovernmental Panel on Climate Change.
- McGregor, J.L., H.B. Gordon, I.G. Waterson, M.R. Dix, and L.D. Rotstayn. 1993. The CSIRO 9-level Atmospheric Circulation Model. 26, CSIRO Division of Atmospheric Research Tech. Paper 26. CSIRO, Mordialloc, VIC, Australia.
- Milly, P.C.D. 1985. A mass-conservative procedure for time-stepping in models of unsaturated flow. *Adv. Water Resour.* 8:32–36.
- Monteith, J.L., and M.H. Unsworth. 1990. Principles of environmental physics. Routledge, Chapman and Hall, New York.
- Overgaard, J., D. Rosbjerg, and M.B. Butts. 2006. Land-surface modelling in hydrological perspective: A review. *Biogeosciences* 3:229–241.
- Peck, A.J., and D.R. Williamson. 1987. Effects of forest clearing on groundwater. *J. Hydrol.* 94:47–65.
- Richardson, C.W., and D.A. Wright. 1984. WGEN: A model for generating daily weather variables. ARS-8. USDA-ARS, Washington, DC.
- Ross, P.J., and K.L. Bristow. 1990. Simulating water movement in layered and gradational soils using the Kirchoff Transform. *Soil Sci. Soc. Am. J.* 54:1519–1524.
- Salas, J.D. 1992. Analysis and modelling of hydrologic time series. p. 72. *In* D.R. Maidment (ed.) *Handbook of hydrology*. McGraw-Hill, New York.
- Scibek, J., and D.M. Allen. 2006. Comparing modelled responses of two high-permeability, unconfined aquifers to predicted climate change. *Glob. Planet. Change* 50:50–62.
- Short, D.L., W.R. Dawes, and I. White. 1996. The practicability of using Richards' equation for general purpose soil-water dynamics models. *Environ. Int.* 21:723–730.
- Sophocleous, M. 2004. Climate change: Why should water professionals care? *Ground Water* 42:637.
- Taniguchi, M. 2002. Estimations of the past groundwater recharge rate from deep borehole temperature data. *Catena* 48:39–51.
- Vertessy, R.A., T.J. Hatton, R.J. Benyon, and W.R. Dawes. 1996. Long term growth and water balance predictions for a mountain ash (*Eucalyptus regnans*) forest catchment subject to clearfelling and regeneration. *Tree Physiol.* 16:221–232.
- Watson, R.T., M.C. Zinyowera, and R.H. Moss (ed.). 1996. Climate change 1995, impacts, adaptations, and mitigation of climate change: Scientific-technical analyses. Contribution of Working Group II to the Second Assessment of the Intergovernmental Panel on Climate Change. Cambridge Univ. Press, Cambridge, UK.
- Watson, R.T., M.C. Zinyowera, and R.H. Moss (ed.). 1998. The regional impacts of climate change: An Assessment of Vulnerability. A Special Report of IPCC Working group II. Cambridge Univ. Press, Cambridge, UK.
- WAWA. 1987. Perth urban water balance study. Vol. 1. Findings. Water Authority of Western Australia, Perth, WA.
- Wessolek, G., and S. Asseng. 2006. Trade-off between wheat yield and drainage under current and climate change conditions in northeast Germany. *Eur. J. Agron.* 24:333–342.
- Whetton, P.H., A.B. Pittock, J.C. Labraga, A.B. Mullan, and A. Joubert. 1996. Southern hemisphere climate: Comparing models with reality. *In* T.W. Giambelluca and A. Henderson-Sellers (ed.) *Climate change: Developing southern hemisphere perspectives*. John Wiley & Sons, New York.
- Wilks, D.S. 1992. Adapting stochastic weather generation algorithms for climate change studies. *Clim. Change* 22:67–84.
- Williamson, D.R., R.A. Stokes, and J.K. Ruprecht. 1987. Response of input and output of water and chloride to clearing for agriculture. *J. Hydrol.* 94:1–28.
- Wu, H., E.J. Rykiel, T. Hatton, and J. Walker. 1994. An integrated rate methodology (IRM) for multi-factor growth rate modelling. *Ecol. Model.* 73:97–116.
- Xu, C.-y., E. Widen, and S. Halldin. 2005. Modelling hydrological consequences of climate change: Progress and challenges. *Adv. Atmos. Sci.* 22:789–797.
- Zhang, L., W.R. Dawes, and T.J. Hatton. 1996. Modelling hydrologic processes using a biophysically based model: Application of WAVES to FIFE and HAPEX-MOBILHY. *J. Hydrol.* 185:147–169.
- Zuppi, G.M., and E. Sacchi. 2004. Hydrogeology as a climate recorder: Sahara-Sahel (north Africa) and the Po Plain (northern Italy). *Glob. Planet. Change* 40:79–91.